Volume 9 | Number 7 | 7 April 2025

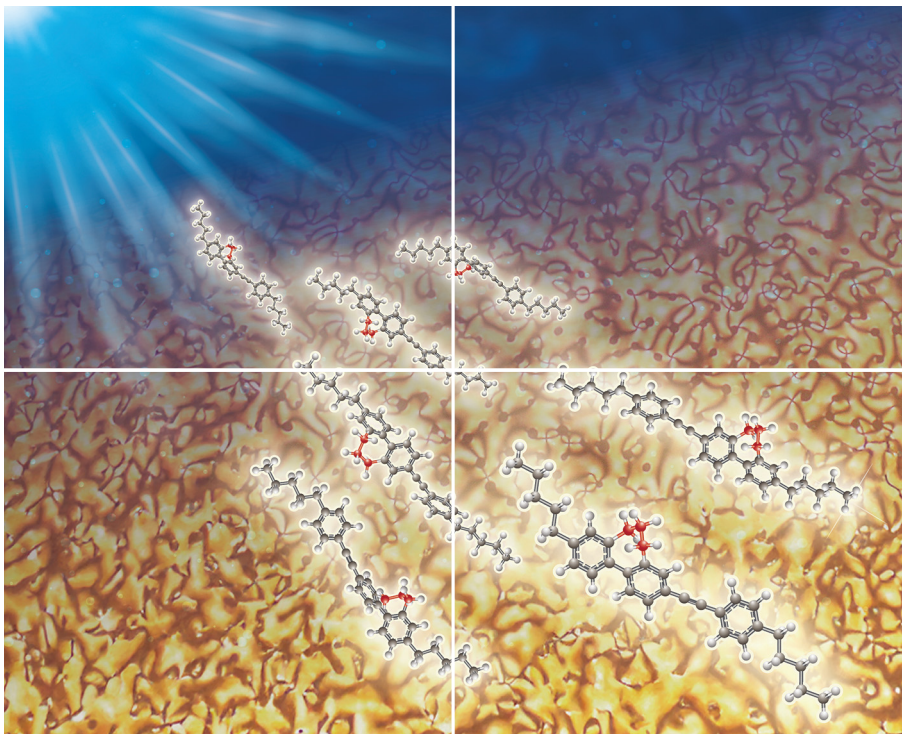

MATERIALS CHEMISTRY

FRONTIERS

CCS 中国化学会 CHINESE CHEMICAL SOCIETY

ICCAS 1956

ROYAL SOCIETY OF CHEMISTRY

rsc.li/frontiers-materials

MATERIALS CHEMISTRY
FRONTIERS

RESEARCH ARTICLE

View Article Online
View Journal | View Issue

Cite this: *Mater. Chem. Front.*, 2025, **9**, 1127

Innovative molecular design of bridged biphenyls for calamitic nematic liquid crystals with extensive π-conjugated mesogens†

Yoshimichi Shimomura,[a] Yuuto Iida,[a] Eiji Tsurumaki [b] and Gen-ichi Konishi *[a]

Received 19th December 2024,
Accepted 13th February 2025

DOI: 10.1039/d4qm01116c

rsc.li/frontiers-materials

To develop advanced materials based on calamitic nematic liquid crystals, it is essential to design functional optoelectronic mesogens that can form nematic phases at low temperatures. This study proposes a new molecular design strategy for low-temperature nematic liquid crystals using large π-conjugated mesogens with optical/electrical functions. Bridged biphenyls were synthesized by bridging the two phenyl rings with propylene. This bridging structure reduced the molecular planarity and prevented the molecules from aligning neatly in one direction, resulting in lowering the temperature range of the nematic phases. Terphenyl and phenyltolane derivatives exhibited supercooled nematic phases at room temperature, while quarterphenyl and bis(phenylethynyl)-biphenyl derivates exhibited nematic phases below 100 °C. The proposed design is more effective for rigid mesogens compared to conventional calamitic nematic liquid crystal design.

Introduction

Since their discovery, calamitic nematic liquid crystals (NLCs) have been intensively investigated owing to their unique properties, including electrical, magnetic, and optical anisotropy, as well as high fluidity.[1] In recent years, new nematic phases as the chiral nematic (cholesteric),[2–6] twist-bend,[7–10] biaxial,[11] blue,[12–14] splay nematic phases,[15] and ferroelectric structures[16] have been investigated. In addition, there has been the development of unique liquid crystal molecules which have a nematic phase.[17–28] From a materials viewpoint, calamitic NLCs are used in liquid crystal displays[29,30] and other functional materials, such as optical films[31–34] and distributed-feedback lasers.[35–39] These applications exploit the anisotropy and fluidity of liquid crystals. Additionally, molecules with optical/electrical functions within the liquid crystals are also gaining significant attention, leading to the development of calamitic NLCs with large π-conjugated systems.[40–45] More sophisticated materials and devices, such as dye-doped high-speed fluorescent switching devices[46–51] and liquid-crystalline organic semiconductors,[52–55] are currently being studied. In general, the nematic phase temperature range of π-conjugated liquid crystals with optical/electrical functions is often too high owing to the high melting point of the mesogen itself and strong intermolecular interactions resulting from their rigid skeletons and functional groups.[56–58] Extending the hydrocarbon chains in the tail to lower this temperature range tends to promote the formation of smectic phases.[59,60]

The most common approach to addressing this issue is to introduce fluorine into the lateral position of mesogens.[61] This method has been effective, as some terphenyl and phenyltolane molecules form a nematic phase below 100 °C due to fluorine incorporation.[23,40] However, introducing fluorine can sometimes alter the electronic states of the original molecules, significantly changing their optical and electrical properties.[24,61–63] Other molecular design strategies include introducing a substituent larger than fluorine and using branch chains in the tail.[64–67] Nevertheless, a new molecular design strategy that can be applied to various mesogens with optical and electrical functions is required for further development of calamitic NLCs.

Very recently, we reported π-extended bridged stilbenes that exhibited nematic phases at near room temperature with luminescence properties.[68] Bridged stilbenes have the 7-membered ring structure that connects the vinyl group and the phenyl ring of stilbenes with a propylene group, referred to as the 'bridging structure.' The flexible bridging structure promoted the intramolecular rotation and the bending motion of the π-conjugated skeletons, enabling the formation of various conformations. This increased the phase-transition entropies and contributed to the lowering of the temperature range of the nematic phase.

[a] *Department of Chemical Science and Engineering, Institute of Science Tokyo, Ookayama, Meguro-ku, Tokyo 152-8552, Japan. E-mail: konishi.g.aa@m.titech.ac.jp*
[b] *Department of Chemistry, Institute of Science Tokyo, Ookayama, Meguro-ku, Tokyo 152-8552, Japan*

† Electronic supplementary information (ESI) available: DSC charts, POM figures, absorption and fluorescence spectra, synthetic procedures, NMR and mass charts, crystallographic analysis. CCDC 2410034. For ESI and crystallographic data in CIF or other electronic format see DOI: https://doi.org/10.1039/d4qm01116c

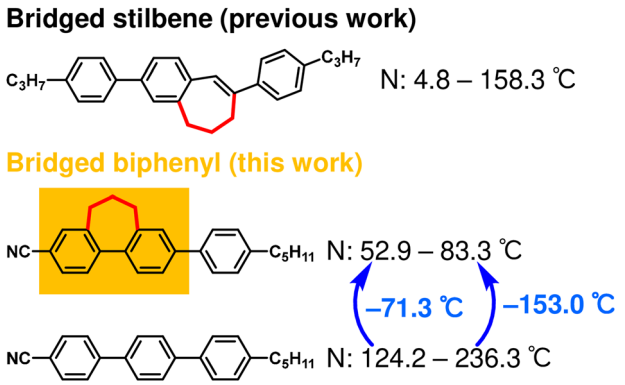

Fig. 1 The conceptual image of the bridged stilbene and the bridged biphenyl.

In this study, we synthesized bridged biphenyls by introducing a bridging structure to biphenyls, which are more common mesogens compared to stilbenes (Fig. 1).

Additionally, we developed biphenyl, terphenyl, quarterphenyl, phenyltolane, and bis(phenylethynyl)-biphenyl-type molecules. Terphenyl- and phenyltolane-type molecules that formed a nematic phase, even at room temperature, were obtained. Additionally, we achieved nematic phases below 100 °C with quarterphenyl and bis(phenylethynyl)-biphenyl molecules. The effect of the bridging structure in the bridged biphenyl also investigated and found to differ from that in the bridged stilbene. Despite this difference, the molecular design strategy of introducing a bridging structure proved superior to previous strategies in terms of lowering the nematic phase temperature range and applicability to large π-conjugated molecules.

Results and discussion

Synthesis and characterization

We synthesized biphenyl, terphenyl, quarterphenyl, phenyltolane, and bis(phenylethynyl)-biphenyl derivatives containing bridged biphenyl by introducing alkyl cyclic structure into biphenyl. For comparison, we synthesized a terphenyl derivative with two methyl groups introduced into the mesogen. The chemical structures of the molecules used in this study are shown in Fig. 2. The synthesis procedures for seven-membered bridged biphenyl, **Bc5CT[7]**, and **B5CT[7]** are illustrated in Scheme 1, and those for the other final products are shown in Schemes S3–S5 (ESI†).

Seven-membered bridged biphenyl was synthesized from 2-formylphenylboronic acid (**1**) and 2′-bromoacetophenone (**2**) using Suzuki–Miyaura cross-coupling reaction, intermolecular aldol condensation and reduction by triethylsilane in a trifluoro acetate solution.[69] The cyano group was introduced through the formylation of the bromo group, followed by treatment with iodine and ammonia.[70] The alkoxy group was formed by first converting the bromo group to a boronate, then reducing it with *m*-chloroperoxybenzoic acid, and finally performing a Williamson ether reaction. Alkylation of the bromo group was achieved using a B-alkyl Suzuki–Miyaura cross-coupling reaction with 9-BBN.[71] Terphenyl and quarterphenyl derivatives were synthesized from the corresponding bridged biphenyl derivatives and arylboronic acids *via* Suzuki–Miyaura cross-coupling.[72–74] Phenyltolane and bis(phenylethynyl)biphenyl derivatives were synthesized from the corresponding bridged biphenyl derivatives and 4-ethynyl aryl *via* Sonogashira cross-coupling.[24]

The synthesized compounds were identified using ^{1}H-NMR, ^{13}C-NMR, and HR-EI spectroscopies. FT-IR spectroscopy was used for molecules with cyano groups.

Phase transition behaviours

The phase transition behaviors of the synthesized compounds were evaluated using DSC and POM. Using POM, we observed the phase transition of the compounds during cooling and heating at a rate of 10 °C min^{-1} for a molten sample sandwiched between untreated glass plates. The phase transition

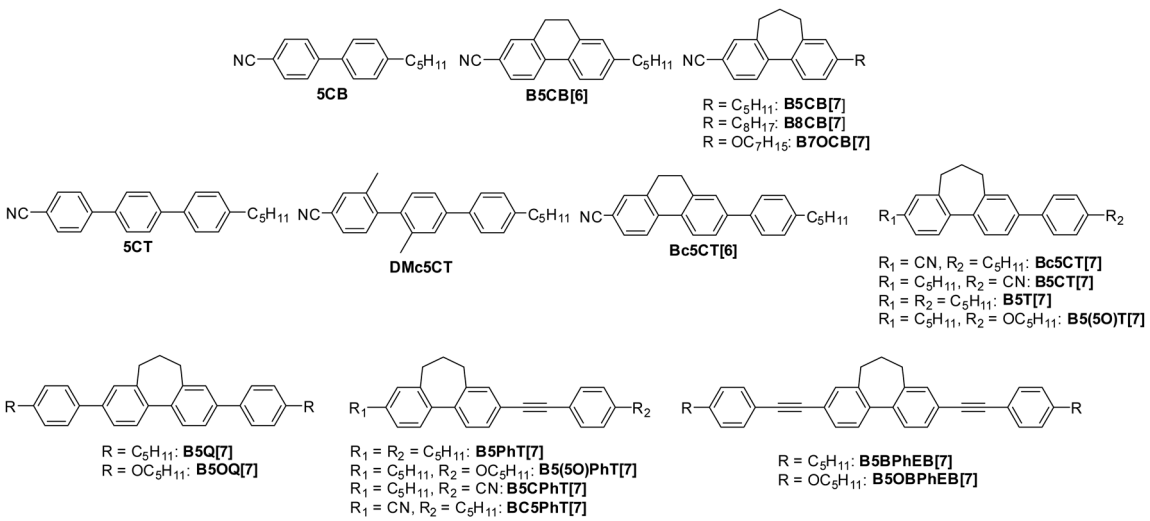

Fig. 2 The molecules list of this research.

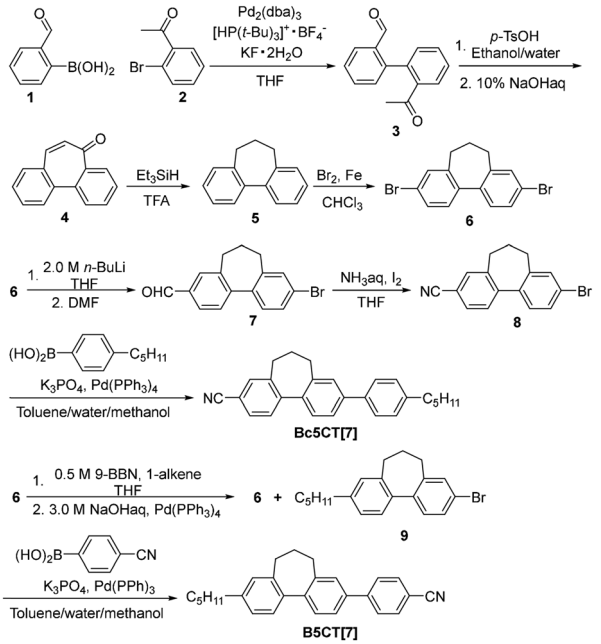

Scheme 1 Synthesis of **Bc5CT[7]** and **B5CT[7]**.

temperatures and enthalpies of synthesized molecules, **5CB**, and **5CT** during the second heating/cooling process are listed in Table 1. The bar graphs of the phase transition temperatures and ranges are shown in Fig. 3. The DSC thermograms are provided in Fig. 4a, 5a, and ESI.†

Phase transition behaviours of biphenyl derivatives. B5CB[6] exhibited endothermic peaks at 5.6 and 43.5 °C, as well as an exothermic peak at 31.5 °C in the heating DSC thermogram (Fig. S2, ESI†). The peaks at 31.5 °C and 43.5 °C overlapped, preventing the calculations of their ΔH values. In contrast, in the cooling DSC thermogram, only one exothermic peak at 3.7 °C was observed. When the sample of **B5CB[6]** was rapidly cooled from 100 to 0 °C by an ice water bath, a schlieren-like texture was observed by POM. But the proper POM image could not be taken because the texture was changed quickly after removal from the bath. The WAXD measurement of **B5CB[6]** could also not be performed due to having no appropriate equipment. We considered this phase to be smectic C because of its no fluidity, even though the ΔH were very small (= 0.4 kJ mol^{-1}). The crystallization continued when the sample was left at room temperature (Fig. S3, ESI†).

None of the seven-membered bridged biphenyl derivatives exhibited phase transitions in the DSC thermograms (Fig. S4, S5, and S7, ESI†). **B5CB[7]** maintained a dark field, **B8CB[7]** formed a schlieren texture (Fig. S6, ESI†), and **B7OCB[7]** crystallized when each prepared slide was left at room temperature for a few days (Fig. S8, ESI†). The schlieren texture of **B8CB[7]** exhibited no fluidity; thus, this phase is smectic C.

Bridged biphenyl derivatives did not show a nematic phase, unlike **5CB**. These results were attributed to multiple factors, such as the steric hindrance of the bridging moiety, decrease in the planarity of the biphenyl, and absence of a biaryl rotational axis.

Terphenyl derivatives: DMc5CT, Bc5CT[6], Bc5CT[7], and B5CT[7]. DMc5CT did not form a liquid crystalline phase. The DSC thermograms of **DMc5CT** exhibited one endothermic peak and one exothermic peak during heating (Fig. 4a). Additionally, one endothermic peak was observed during cooling. In POM, **DMc5CT** exhibited only a crystalline phase (Fig. 4b and c).

Table 1 Phase transition behaviours of the compounds, determined by DSC measurement at a rate of 10 °C min^{-1} upon 2nd heating and cooling

	Phase transition temperature [°C] (enthalpy [kJ mol^{-1}])	
Entry	Heating	Cooling
5CB	N 35.8 (0.6) Iso	Iso 33.8 (−0.6) N
B5CB[6]	SmC 5.6 (0.4) Iso 31.5 (—) Cry 43.4 (—) Iso	Iso 3.7 (−0.4) SmC
B5CB[7]	—	—
B8CB[7]	—	—[a]
B7OCB[7]	—	—[a]
5CT	Cry$_1$ 105.6 (0.8) Cry$_2$ 130.9 (10.6) N 238.2 (1.2) Iso	Iso 236.3 (−1.1) N 126.8, 124.2 (−10.0) Cry$_1$
DMc5CT	Cry$_1$ −5.9 (−0.5) Cry$_2$ 84.0 (23.7) Iso	Iso 9.3 (−15.4) Cry$_1$
Bc5CT[6]	N 43.6, 59.0 (−18.6) Cry 113.5 (28.3) N 208.4 (1.0) Iso	Iso 206.6 (−0.9) N
Bc5CT[7]	Cry$_1$ 36.0 (−7.7) Cry$_2$ 67.6 (−3.2) Cry$_3$ 120.7 (28.7) Iso	Iso 83.3 (−1.4) N 52.9 (−3.8) Cry$_1$
B5CT[7]	—	—[a]
B5T[7]	N 10.9 (0.25) Iso	Iso 8.9 (−0.2) N
B5(5O)T[7]	N 18.1 (−15.8) Cry 50.2 (21.5) N 59.7, 61.6 (2.2) Iso	Iso 57.6 (−0.5) N
B5Q[7]	Cry 142.6 (32.2) N 178.4 (1.0) Iso	Iso 176.3 (−1.1) N 82.4 (−26.3) Cry
B5OQ[7]	Cry 164.6 (40.9) N 229.2 (1.3) Iso	Iso 227.3 (−1.3) N 136.4 (−41.1) Cry
B5PhT[7]	N 49.2 (0.9) Iso	Iso 47.0 (−1.0) N
B5(5O)PhT[7]	N 36.2 (−23.2) Cry 78.9 (31.7) N 94.6 (1.4) Iso	Iso 92.5 (−2.0) N
BC5PhT[7]	Cry 132.2 (25.9) Iso	Iso 130.7 (−1.2) N 115.6 (−22.9) Cry
B5CPhT[7]	N 101.1 (0.3), 104.9 (0.6) Iso	Iso 102.4 (0.9) N
B5BPhEB[7][b]	Cry 120 N 240 Iso	Iso 237 N 52 Cry
B5OBPhEB[7][b]	Cry 150 N 260 Iso	Iso 254 N113 Cry

[a] There were no peak in DSC thermogram and no phase transition in POM observation at a rate of 10 °C min^{-1}, but **B8CB[7]** and **B7OCB[7]** showed a smectic C and a crystalline phase at room temperature after a few days in POM observation, respectively. On the other hand, **B5CT[7]** exhibited an isotropic–nematic phase transition after a few minutes and a gradual nematic–crystalline phase transition after a few more days at room temperature. [b] Phase transition temperatures were determined by POM.

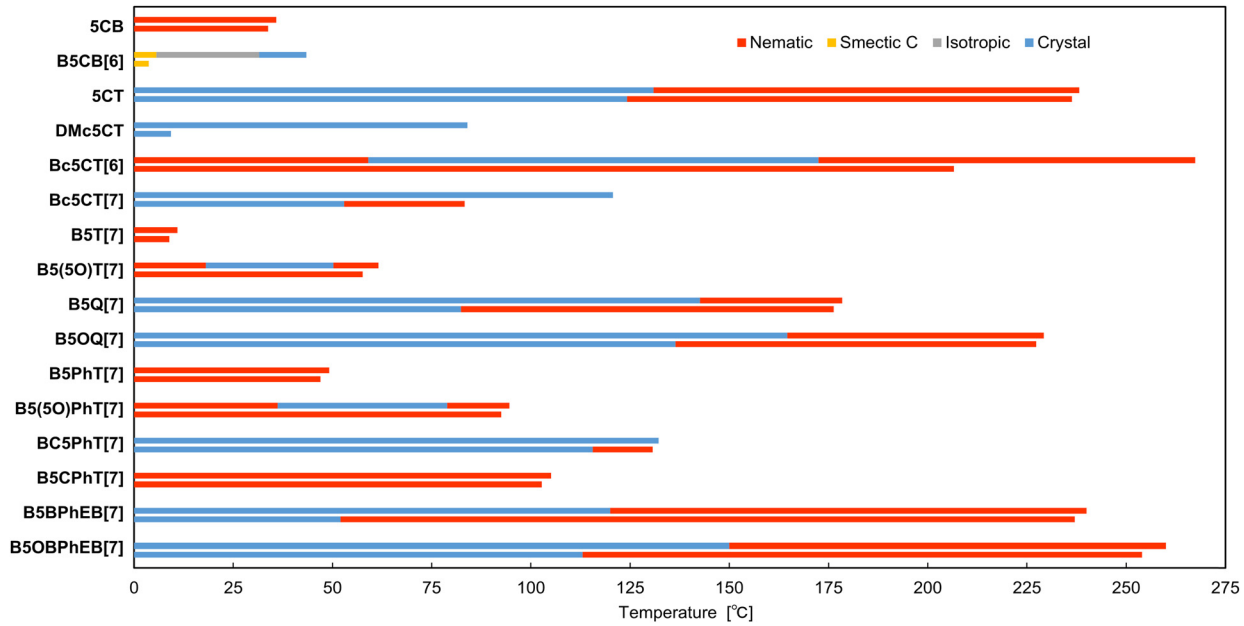

Fig. 3 Schematic diagram showing the phase transition temperatures and ranges of the compounds, except for **B5CB[7]**, **B8CB[7]**, **B7OCB[7]**, and **B5CT[7]**; upper bar: upon heating, lower bar: upon cooling.

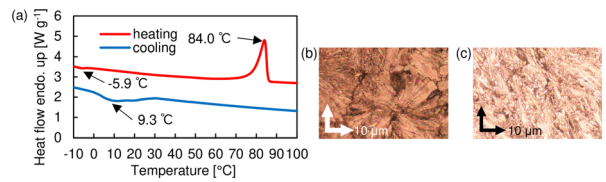

Fig. 4 (a) DSC thermograms of **DMc5CT** at a rate of 10 °C min^{-1} upon 2nd heating and cooling, and POM images of **DMc5CT** at (b) 0 °C during cooling and (c) room temperature left for a few days.

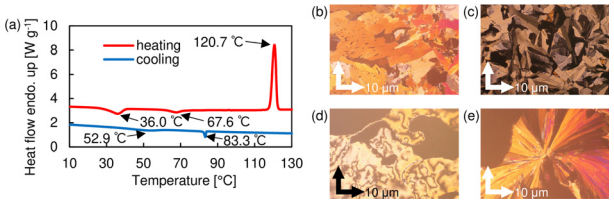

Fig. 5 (a) DSC thermograms of **Bc5CT[7]** at a rate of 10 °C min^{-1} upon 2nd heating and cooling, and POM images of **Bc5CT[7]** at (b) 40 °C during heating, (c) 70 °C during heating, (d) 70 °C during cooling, and (e) 40 °C during cooling.

The large steric hindrance and torsion of the mesogen by the methyl groups inhibit the formation of liquid crystalline phases.

Bc5CT[6] formed an enantiotropic nematic phase. The DSC thermograms exhibited two exothermic peaks at 43.6 and 59.0 °C and two endothermic peaks at 113.5 and 208.4 °C during heating, while only one exothermic peak was observed at 206.6 °C during cooling (Fig. S10, ESI†). POM observations revealed that **Bc5CT[6]** exists in a nematic phase (Fig. S11b, ESI†). A gradual nematic-to-crystalline phase transition was observed at 40 °C (Fig. S11c, ESI†). The crystallization rate of **Bc5CT[6]** was lower than that of **5CT**. In particular, the lower temperature limit of the nematic phase during cooling was significantly reduced.

In contrast, **Bc5CT[7]** formed a monotropic nematic phase, showing two exothermic peaks and one endothermic peak during heating and two exothermic peaks during cooling in the DSC thermograms (Fig. 5a). In POM, a nematic phase was observed between the two exothermic peaks during cooling (Fig. 5d). Moreover, unlike **Bc5CT[6]**, **Bc5CT[7]** exists in at least three different crystalline phases (Fig. 5b, c and e). The isotropic-to-nematic and the nematic-to-crystalline phase transition temperatures of **Bc5CT[7]** are below at 153.0 °C and 71.5 °C compared to those of **5CT**, respectively.

B5CT[7], with a different bridge position from **Bc5CT[7]**, exhibited no phase transition peak during heating at a rate of 10 °C min^{-1} (Fig. S12, ESI†). When the prepared slide of the once-melted **B5CT[7]** was left at room temperature for a few minutes, the isotropic–nematic phase transition proceeded, and the nematic–crystalline phase transition developed gradually after a few more days (Fig. S13, ESI†). This indicates that steric hindrance of the bridging moiety inhibit crystallization. The crystallized **B5CT[7]** transitioned to an isotropic phase at 86.7 °C upon heating at a rate of 10 °C min^{-1} in POM.

The diversity of crystalline systems due to the bridging structure and the associated significant reduction in the phase transition temperatures occurred, which is also common to the stilbene and distyrylbenzene dyes we have previously reported.[68,75–78] This result suggests that the molecular design strategy of the seven-membered bridging is effective for the

development of calamitic liquid crystals with a nematic phase near room temperature. The effect of the bridging structure in the bridged biphenyl is discussed later.

B5T[7] and B5(5O)T[7]. **B5T[7]** exhibited an enantiotropic nematic phase. One endothermic and exothermic peaks below room temperature were observed in the heating and cooling DSC thermograms, respectively (Fig. S14, ESI†). Immediate POM observations revealed a nematic phase after cooling the prepared slide to 0 °C (Fig. S15, ESI†).

B5(5O)T[7] also exhibited an enantiotropic nematic phase, with one exothermic peak and three endothermic peaks during heating. Moreover, it exhibited one exothermic peak during cooling in the DSC thermograms (Fig. S16, ESI†) and a schlieren texture (Fig. S17b and c, ESI†). **B5(5O)T[7]** maintained the nematic phase after cooling to 0 °C at a rate of 10 °C min^{-1} and underwent cold crystallization upon heating to 20 °C, as indicated by a broad peak, indicating the remarkable effect of the seven-membered bridging structure. Prepared slide of **B5(5O)T[7]** transitioned from the nematic to the crystalline phase when left at room temperature for a few minutes (Fig. S17a, ESI†). There were two exothermic peaks near the nematic to isotropic phase transition during heating, indicating that a nematic–nematic phase transition would occur. However, we could not observe any event in POM and could not conduct the WAXD measurement in this temperature range as it was only 1.9 °C. Therefore, this is not discussed in detail.

Regardless of the substituents, the seven-membered bridging structure contributed significantly to the reduction in the temperature range of the nematic phase. The results of applying this molecular design strategy to even larger π-conjugated molecules are presented below.

Quarterphenyl derivatives: B5Q[7] and B5OQ[7]. Both **B5Q[7]** and **B5OQ[7]** are enantiotropic nematic liquid crystals, and their DSC thermograms exhibited two endothermic and exothermic peaks during heating and cooling, respectively (Fig. S18 and S20, ESI†). Moreover, they exhibited schlieren textures in the temperature range between these peaks (Fig. 6a and Fig. S21, ESI†). The temperature ranges of the nematic phase of **B5Q[7]** were 142.6–178.4 °C and 176.3–82.4 °C in heating and cooling, and those of **B5OQ[7]** were 164.6–229.2 °C and 227.3–136.7 °C, respectively. **B5OQ[7]** has a higher phase transition temperature than **B5Q[7]** because of the increased intermolecular interactions with the O atoms.

Phenyltolane derivatives. **B5PhT[7]** is a nematic liquid crystal. The DSC measurements revealed only one peak during heating and cooling (Fig. S22, ESI†). Additionally, in the POM observations, a schlieren texture was evident at room temperature (Fig. 6b). At a cooling rate of 10 °C min^{-1}, **B5PhT[7]** did not crystallize, and the nematic phase was retained even after the prepared slide used for POM observation was left at room temperature for several weeks. Such a thermodynamically stable nematic phase at room temperature from a single compound is quite rare.

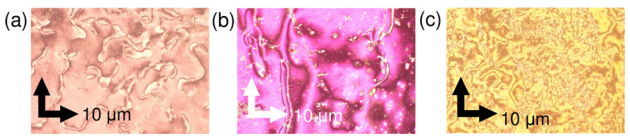

Fig. 6 POM images of (a) **B5Q[7]** at 100 °C during cooling, (b) **B5PhT[7]** at room temperature, and (c) **B5BPhEBT[7]** at 80 °C during cooling.

B5(5O)PhT[7] exhibited an enantiotropic nematic phase with phase transition behavior similar to **B5(5O)T[7]** (Fig. S23, ESI†). The phase transition temperatures of **B5(5O)PhT[7]** increased by 18–35 °C compared to those of **B5(5O)T[7]**. In the POM observations, a schlieren texture was observed, and the nematic-to-isotropic phase transition of **B5(5O)PhT[7]** occurred over a period of 15 minutes at room temperature (Fig. S24, ESI†).

BC5PhT[7] formed a monotropic nematic phase, and its DSC thermograms exhibited an endothermic peak at 133 °C during heating. Additionally, two exothermic peaks at 131 and 116 °C during cooling were observed (Fig. S25, ESI†). Under POM, **BC5PhT[7]** exhibited a schlieren texture between the two exothermic peak temperatures (Fig. S26, ESI†).

On the other hand, **B5CPhT[7]** exhibited a nematic phase; the nematic ⇄ isotropic phase transition temperatures during heating and cooling were 105 and 103 °C, respectively (Fig. S27, ESI†). Moreover, the nematic-to-nematic phase transition was also observed on heating in the DSC chart. However, this is not discussed in detail for the same reason as for **B5(5O)T[7]**. While **B5CPhT[7]** did not show any crystallization peak in the DSC measurement despite cooling to 0 °C, the prepared **B5CPhT[7]** crystallized when left at room temperature for a few minutes (Fig. S28, ESI†). Although the crystallization temperature was not determined, this crystalline phase melted at 100.0 °C and transitioned to the nematic phase.

Unlike **B5CPhT[7]**, where the bridge is located near the pentyl group, **BC5PhT[7]**, where the bridge is situated near the cyano group, crystallized on a time scale of 10 °C min^{-1}. This trend was also observed for terphenyl derivatives. This can be attributed to the significantly increased flexibility of the molecules due to the proximity of the pentyl chains and bridging structures. The cause of this phenomenon remains unclear, and the molecular alignments were not determined. This will be explored in future investigations.

Bis(phenylethynyl)-biphenyl derivatives. The phase transition temperatures of the bis(phenylethynyl)-biphenyl derivatives were determined by POM, because their prepared samples discoloured from colourless to brown when heated on a hot-stage just below their clearing points. DSC measurements were not conducted due to suspected sample decomposition.

The bis(phenylethynyl)-biphenyl derivatives transitioned from colorless to brown upon heating to their isotropic phases. In particular, **B5BPhEB[7]** exhibited an enantiotropic nematic phase, displaying a schlieren texture at 120–240 °C and 237–52 °C during heating and cooling, respectively (Fig. 6c and Fig. S29, ESI†). **B5OBPhEB[7]** also exhibited an enantiotropic nematic phase at 150–260 °C and 254–113 °C during heating and cooling, respectively (Fig. S30, ESI†).

The use of the seven-membered bridging molecular design strategy has enabled these large π-conjugated molecules to

successfully form nematic phases at temperatures below 100 °C, and some terphenyl and phenyltolane derivatives exhibited nematic phases at room temperature. Even in very rigid skeletons such as quaterphenyl and bis(phenylethynyl)-biphenyl, this strategy was effective in lowering the nematic phase temperatures.

Birefringence

To investigate the effect of the bridge structure on the birefringence, we measured the temperature dependence of birefringence (Δn) for **5CT** and **Bc5CT**[7] in the nematic phases, using the method described in our previous report.[79–81] However, **Bc5CT**[7] crystallized during the measurement process, thus we conducted measurements for quarterphenyl and bis(phenylethynyl)-biphenyl derivatives, whose mesogens consist of large π-conjugated skeletons.

This study followed the general practice of indexing the temperature dependence properties in nematic phases to the reduced temperature ($T_{IN} - T$), where T_{IN} is the isotropic-to-nematic phase transition temperature, and T is the measurement temperature. Fig. 7a compares the dependence of the Δn at 550 nm on $T_{IN} - T$ for **5CT**, **B5Q**[7], **B5OQ**[7], **B5BPhEB**[7], and **B5OBPhEB**[7]. Quarterphenyl and bis(phenylethynyl)-biphenyl derivatives with the bridging structure exhibited larger Δn than that of **5CT** at the same $T_{IN} - T$ value, despite **5CT** having a cyano group at the end. Among the same mesogens, **B5OQ**[7] and **B5OBPhEB**[7] exhibited larger Δn than that of **B5Q**[7] and **B5BPhEB**[7], respectively, owing to the polarizability of terminal groups in the following order: alkoxy group > alkyl group. In addition, these results were applied to the empirical Haller's equation[82] for further detailed analysis in nematic phases. The empirical Haller's equation is as follows;

$$S = \Delta n/\Delta n_0$$

$$\Delta n = \Delta n_0 \, (1 - T/T_{IN})^{\beta}$$

where S is the order parameter, Δn_0 is Δn at $S = 1$, and β is a constant. The values of S and Δn at $T_{IN} - T = 15$ °C, as well as Δn_0 and β are summarized in Table 2, and the $T_{IN} - T$ dependance of S is shown in Fig. 7b. The trend of Δn_0 was similar to that of the Δn; however, the Δn_0 value of **B5OQ**[7] was smaller than that of **B5Q**[7]. Focusing on S and β, the values of **5CT** and **B5Q**[7] were nearly identical. In contrast, the S values of **B5OQ**[7], **B5BPhEB**[7], and **B5OBPhEB**[7] were very large (>0.70), and their β values were very small (<0.10); typical

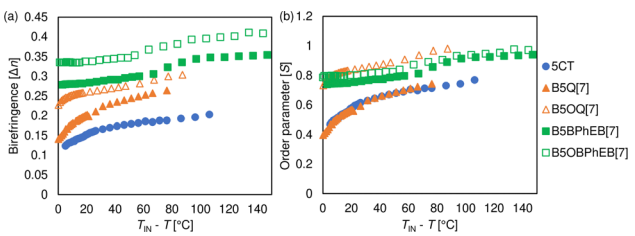

Fig. 7 (a) Δn and (b) ΔS of **5CT** (●), **B5Q**[7] (▲), **B5OQ**[7] (△), **B5BPhEB**[7] (■), and **B5OBPhEB**[7] (□) at each $T_{IN} - T$.

Table 2 Experimental Δn values, as well as extrapolated parameters for **5CT**, **B5Q**[7], **B5OQ**[7], **B5BPhEB**[7], and **B5OBPhEB**[7] at $T_{IN} - T = 15$ °C

Compound	Δn^a	$\Delta n_0{}^b$	S^a	β^b
5CT	0.15	0.26	0.54	0.17
B5Q[7]	0.20	0.36	0.54	0.18
B5OQ[7]	0.26	0.31	0.83	0.05
B5BPhEB[7]	0.29	0.38	0.75	0.08
B5OBPhEB[7]	0.34	0.42	0.80	0.06

[a] At $T_{IN} - T = 15$ °C. [b] Extrapolated by fitting to Haller's equation.

calamitic NLCs have β values of approximately 0.20. **B5OQ**[7], **B5BPhEB**[7], and **B5OBPhEB**[7] exhibited a sudden increase of Δn values when the temperature difference $T_{IN} - T$ was approximately 60 °C, while **B5BPhEB**[7] and **B5OBPhEB**[7] exhibited no Δn increase when the $T_{IN} - T$ was less than 30 °C. This indicates that the Δn_0 values of **B5OQ**[7], **B5BPhEB**[7], and **B5OBPhEB**[7] may not be accurate. Conversely, those of **5CT** and **B5Q**[7] were accurately measured. Considering the facts that the Δn value of **B5Q**[7] was larger than that of **5CT** at each $T_{IN} - T$, and the S value of **B5Q**[7] was almost the same as that of **5CT**, the bridging structure does not seem to have a significant effect on the birefringence and the order parameter in nematic phases.

Photophysical properties

The photophysical properties of **B5PhT**[7] and **B5(5O)PhT**[7], which exhibit nematic phases at room temperature, were measured in dilute solution, their solid states, and nematic phases (Table 3). Their absorption and fluorescence spectra are depicted in Fig. 8.

The absorption spectrum of **B5PhT**[7] in THF solution exhibits a vibrational structure with peaks (the absorption wavelength, λ_{abs}) at 304 nm (max) and 321 nm (Fig. 8a). As indicated in a previous report,[83] the peaks are derived from the $S_0 \rightarrow S_1$ transition. The molar absorption coefficient (ε) was 47 000 M^{-1} cm^{-1}. The fluorescence spectrum of **B5PhT**[7] in THF also shows a vibrational structure, and the fluorescence wavelengths (λ_{fl}) are 346 nm and 359 nm (max). The λ_{fl} of **B5PhT**[7] in the solid state are 365 nm and 408 nm, and the longer λ_{fl} is red-shifted by 50 nm compared to that in THF. The λ_{fl} values in the nematic phase are almost identical to those in the solid state, 363 nm and 406 nm. On the other hand, the maximum λ_{fl} values in these states are different, which are 365 nm and 406 nm in the solid and nematic phases, respectively.

Both of the absorption/fluorescence spectra of **B5(5O)PhT**[7] in THF solution exhibit a vibrational structure similar to those of **B5PhT**[7] (Fig. 8b). The λ_{abs} values are 304 nm and 321 nm (max), and λ_{fl} values are 346 nm (shoulder) and 359 nm, all of which are red-shifted by 5 nm compared to those of **B5PhT**[7]. This can be attributed to the narrowing of the HOMO–LUMO gap by the electro-donating alkoxy group. The fluorescence spectrum in the solid state has a maximum peak at 380 nm and shoulder at 394 nm and that in the nematic phase only shows one peak at 375 nm, which is different from that of

Table 3 Photophysical properties of **B5PhT[7]** and **B5(5O)PhT[7]**

Entry	State	ε [M^{-1} cm^{-1}]	λ_{abs} [nm]	$\lambda_{fl}{}^{ab}$ [nm]
B5PhT[7]	THF	47 000	304 (max), 321	340, 354 (max)
	Solid	—	—	365 (max), 408
	Nematic phase	—	—	353, 406 (max)
B5(5O)PhT[7]	THF	44 000	309 (max), 326	346 (shoulder), 359
	Solid			380, 394 (shoulder)
	Nematic phase			375

[a] Excited at 304 nm for **B5PhT[7]**. [b] Excited at 309 nm for **B5(5O)PhT[7]**.

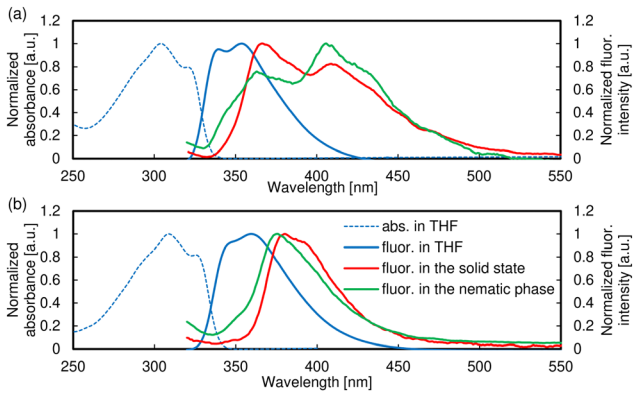

Fig. 8 Absorption (dashed line) and fluorescence (solid line) spectra of (a) **B5PhT[7]** and (b) **B5(5O)PhT[7]**.

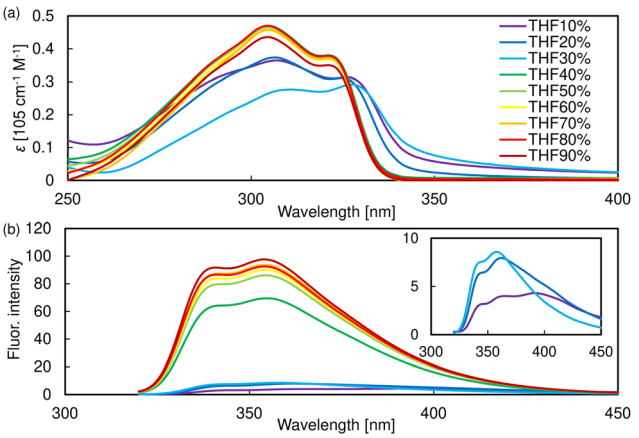

Fig. 9 (a) Absorption and (b) fluorescence spectra of **B5CT[7]** in THF/water mixed solvent at 1.0×10^{-5} M.

B5PhT[7]. The increase in the electronic molecular interaction owing to the alkoxy group is likely to have contributed to this result.

B5PhT[7] exhibits different fluorescence behavior in THF solution, in both the solid and nematic phases. To conduct detailed investigations, we first measured the absorption/fluorescence spectrum of the polymethacrylate (PMMA, M_n = 1 000 000) cast film doped with 0.1 wt% **B5PhT[7]**; however, they are almost the same as those in THF solution (Fig. S36, ESI†). Subsequently, a **B5PhT[7]** agglomeration experiment in a THF/water system was performed, and the aggregation of **B5PhT[7]** could be observed in ≤30% THF suspension. The absorption spectra in ≤30% THF suspension exhibit the decrease in ε and the slight red-shifted longer-wavelength peak (Fig. 9a). The fluorescence spectra in 20% and 30% THF solution also changed slightly, and in THF 10% solution, a fluorescence peak appears at 394 nm, with a spectrum similar to a superposition of those in the THF solution and nematic phase (Fig. 9b). These results suggest that the fluorescence peak near 394 nm was caused by intermolecular interactions. Finally, the fluorescence lifetimes of **B5PhT[7]** in the THF solution, solid state, and nematic phase were measured. Unfortunately, the lifetime in the THF solution could not be measured because it was very short (<1.0 ns) and we did not have the proper wavelength cutting filter or LED laser. However, one of the components in the solid and nematic phase exhibited long lifetimes (solid: 6.8 ns, nematic phase: 12.8 ns), complementing the presence of the fluorescence peak resulting from intermolecular interactions (Table S1 and Fig. S37, ESI†). A single-crystal X-ray structure analysis is effective for further investigations of the fluorescence behavior in the solid and nematic phases, but the single crystal of **B5PhT[7]** was not obtained.

B5PhT[7] and **B5(5O)PhT[7]** show blue luminescence in THF, in their solid and nematic phases. They can be used as liquid crystalline and even optical materials. Furthermore, fluorescent liquid crystals show the potential to be applied for more advanced optoelectronics, such as electric-field-responsive fluorescent switch devices.[68,84,85]

Structural analysis

A single-crystal X-ray analysis of **Bc5CT[7]** was conducted (Fig. 10). **Bc5CT[7]** had two atropisomers, and it formed a γ structure. The torsional angle of the biaryl axis at the bridging part in both conformations was 46.8°, and the intermolecular aromatic carbon distance was 3.53 Å. In this single crystal, the molecular long axis was oriented in two different directions, forming an angle of about 60°. The single-crystal X-ray structure of **5CT** was previously reported.[86] In the single crystal, the molecule was determined to have only one conformation, and the molecular long axis was aligned in one direction (Fig. S38, ESI†). The torsional angle of the biaryl axis and intermolecular aromatic carbon distance of **5CT** were 40.9° and 3.63 Å, respectively.

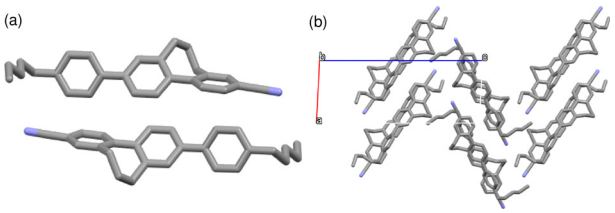

Fig. 10 (a) Molecular conformations and (b) the crystal structure of **Bc5CT[7]** (ESI†).

To investigate the conformation of the bridged biphenyl in more detail, the optimized structure of **BT[7]** was calculated using density functional theory (DFT) at the B3LYP/6-311G(d) level[87] (Fig. 11).

BT[7] showed two optimized structures (Fig. 11b and c). The torsional angle of φ_1 of **Opt-BT[7]-I** and **Opt-BT[7]-II** were 47.8° and 47.3°, respectively, which were 6.6° and 6.1°, respectively, larger than that of biphenyl (φ_1 = 41.2°). These structures were in an atropoisomeric relationship, in which the positions of C_α and C_β relative to the paper plane were reversed, consistent with the results of single-crystal **Bc5CT[7]**.

Calculations of **Opt-BT[7]-I** with φ_1 varying in 5°-steps showed that the rotational energy barrier (E_{bar}) significantly changed around φ_1 = 30° (Fig. 11d). Calculations performed for every 1° φ_1 between 25–35° showed a sudden change at 28–29° (Fig. S43, ESI†). The maximum E_{bar} was 117.8 kJ mol^{-1}, which was much larger than that of biphenyl (9.7 kJ mol^{-1}). The scan calculation had two local minimum values at −50° and 45°, where the structures were almost identical to those of **Opt-Bt[7]-I** and **Opt-BT[7]-II**, respectively (Fig. S41, ESI†). The results of a set of calculations for varying φ_2 are shown in Fig. 11e, and they exhibit a significant change of E_{bar} and two local minimum values, like φ_1. The maximum E_{bar} of φ_2 was about half that of φ_1. Moreover, E_{bar} did not change much around φ_2 = −20–30°. In this angular range, the change of φ_1 was also suppressed (Fig. S45, ESI†). The bridging structure caused this behavior, resulting in the E_{bar} remaining almost constant. Conversely, the structures at each local minimum value were close to those of **Opt-BT[7]-I** and **Opt-BT[7]-II** (Fig. S42, ESI†). In these calculations, there were only two stable conformations of the seven-membered bridged biphenyl. This was different from the case of the bridged stilbenes, which had various conformations.[68] The biaryl axis of the bridged biphenyl was more twisted compared to that of biphenyl. Considering the result of the single-crystal X-ray analysis (ESI†), the decrease in the intermolecular interaction due to the low molecular planarity and difficulty in aligning the molecular long axis in one direction contribute to the lower phase transition temperatures of bridged biphenyl derivatives. This mechanism is different from that of bridged stilbene derivatives, where the increase in the entropy from forming various conformations contributes significantly.

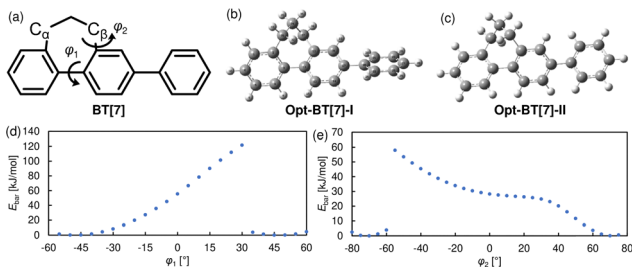

Fig. 11 (a) The chemical structure of **BT[7]**, the conformations of (b) **Opt-BT[7]-I** and (c) **Opt-BT[c]-II**, and E_{bar} of (d) φ_1 and (e) φ_2.

Conclusions

We synthesized biphenyl, terphenyl, quarterphenyl, phenyltolane, and bis(phenylethynyl)-biphenyl derivatives, incorporating a seven-membered bridged biphenyl structure in the mesogens. Except for the biphenyl-type compounds, all compounds formed nematic phases. The nematic phase temperature range of **Bc5CT[7]** was approximately 100 °C lower than that of **5CT**, and it exhibited a nematic phase even at room temperature. In contrast, **DMc5CT** exhibited no liquid crystalline phase. Moreover, some terphenyl/phenyltolane skeleton molecules exhibited nematic phases at or below room temperature. **B5Q[7]** and **B5BPhEB[7]**, whose mesogens are quarterphenyl and bis(phenylethynyl)-biphenyl, respectively, exhibited nematic phases even below 100 °C. These results indicate that the molecular design strategy of seven-membered bridging can potentially solve a long-standing challenge in the field of calamitic NLC research, which continues from Vorländer's research.[88] In this study, we have focused on the phase transition behavior of calamitic molecules with only one bridging introduced. On the other hand, those of calamitic molecules with multiple bridging introduced and the effect of introducing the bridging structure into biphenyl on the nematic phases remain unexplored. We will investigate these unknowns in the future. In addition, functional materials, such as liquid crystalline organic semiconductors and advanced materials,[89–100] will be developed using this molecular design strategy.

Data availability

The data supporting this article have been included as part of the ESI.† Crystallographic data for **Bc5CT[7]** has been deposited at the CCDC under 2410034 and can be obtained from **https://www.ccdc.cam.ac.uk/**.

Conflicts of interest

There are no conflicts to declare.

Acknowledgements

We thank Yuki Sawatari (Department of Chemical Science and Engineering, Institute of Science Tokyo) for the birefringence measurements. We also thank Masato Koizumi (Materials Analysis Division, Institute of Science Tokyo) for the HRMS

measurements. This division is independent of our laboratory to ensure fairness. YS thanks JSPS Research Fellowships for Young Scientists. This project was supported in part by MEXT/JSPS KAKENHI grants 24KJ1084 (YS), 23H02036 (GK), Iketani Science and Technology Foundation (YS), Murata Science and Education Foundation (GK). Tokyo Institute of Technology merged with Tokyo Medical and Dental University to form Institute of Science Tokyo (Science Tokyo) on October 1, 2024.

Notes and references

1 D. Demus, J. Goodby, G. W. Gray, H. W. Spiess and V. Vill, *Physical Properties of Liquid Crystals*, Wiley-VCH, Weinheim, 1999.
2 M. Mitov, Cholesteric Liquid Crystals with a Broad Light Reflection Band, *Adv. Mater.*, 2012, **24**, 6206–6276.
3 G. Friedel, Les états mesomorphs de la matière, *Ann. Phys.*, 1922, **9**, 273–474.
4 M. Ozaki, Y. Matsuhisa, H. Yoshida, R. Ozaki and A. Fuji, Photonic crystals based on chiral liquid crystal, *Phys. Status Solidi A*, 2007, **204**, 3777–3789.
5 Y. He, S. Lin, J. Guo and Q. Li, Circularly polarized luminescent self-organized helical superstructures: From materials and stimulus-responsiveness to applications, *Aggregate*, 2022, **3**, e141.
6 J. Xiang, Y. Li, Q. Li, D. A. Paterson, J. M. D. Storey, C. T. Imrie and O. D. Lavrentovich, Electrically Tunable Selective Reflection of Light from Ultraviolet to Visible and Infrared by Heliconical Cholesterics, *Adv. Mater.*, 2015, **27**, 3014–3018.
7 M. Cestari, S. Diez-Berart, D. A. Dunmur, A. Ferrarinim, M. R. de la Fuente, D. J. B. Jackson, D. O. Lopez, G. R. Luckhurst, M. A. Perez-Jubindo, R. M. Richardson, J. Salud, B. A. Timimi and H. Zimmermann, Phase behavior and properties of the liquid-crystal dimer 1″,7″-bis(4-cyanobiphenyl-4′-yl) heptane: A twist-bend nematic liquid crystal, *Phys. Rev. E: Stat., Nonlinear, Soft Matter Phys.*, 2011, **84**, 031704.
8 P. A. Henderson and C. T. Imrie, Methylene-linked liquid crystal dimers and the twist-bend nematic phase, *Liq. Cryst.*, 2011, **38**, 1407–1414.
9 R. J. Mandle, The dependency of twist-bend nematic liquid crystals on molecular structure: a progression from dimers to trimers, oligomers and polymers, *Soft Matter*, 2016, **12**, 7883–7901.
10 Y. Arakawa, K. Komatsu and H. Tsuji, Twist-bend nematic liquid crystals based on thioether linkage, *New J. Chem.*, 2019, **43**, 6786–6793.
11 R. J. Mandle, N. Sebastián, J. Martinez-Perdiguero and A. Mertelj, On the molecular origins of the ferroelectric splay nematic phase, *Nat. Commun.*, 2021, **12**, 4962.
12 H. Coles and M. Pivnenko, Liquid crystal 'blue phases' with a wide temperature range, *Nature*, 2005, **436**, 997–1000.
13 H. Kikuchi, M. Yokota, Y. Hisakado, H. Yang and T. Kajiyama, Polymer-stabilized liquid crystal blue phases, *Nat. Mater.*, 2002, **1**, 64–68.
14 J. Yang, W. Zaho, W. He, Z. Yang, D. Wang and H. Cao, Liquid crystalline blue phase materials with three-dimensional nanostructures, *J. Mater. Chem. C*, 2019, **7**, 13352–13366.
15 A. Mertelj, L. Cmok, N. Sebastián, R. J. Mandle, R. R. parker, A. C. Whitwood, J. W. Goodby and M. Čopič, Splay Nematic Phase, *Phys. Rev. X*, 2018, **8**, 041025.
16 R. J. Mandle, N. Sebastián, J. Martinez-Perdiguero and A. Mertelj, On the molecular origins of the ferroelectric splay nematic phase, *Nat. Commun.*, 2021, **12**, 4962.
17 S. Kumar and A. N. Gowda, The chemistry of bent-core molecules forming nematic liquid crystals, *Liq. Cryst. Rev.*, 2015, **3**, 99–145.
18 N. Sebastián, M. Čopič and A. Mertelj, Ferroelectric nematic liquid-crystalline phases, *Phys. Rev. E*, 2022, **106**, 021001.
19 T. Ghosh and M. Lehmann, Recent advances in heterocycle-based metal-free calamitics, *J. Mater. Chem. C*, 2017, **5**, 12308–12337.
20 R. Cai and E. T. Sanyksju, New thermotropic liquid crystals derived from thiophenes, *Liq. Cryst.*, 1991, **9**, 616–674.
21 P. Kirsch and M. Bremer, Nematic Liquid Crystals for Active Matrix Displays: Molecular Design and Synthesis, *Angew. Chem., Int. Ed.*, 2000, **39**, 4216–4235.
22 S. A. Hudson and P. M. Maitlies, Calamitic Metallomesogens: Metal-Containing Liquid Crystals with Rodlike Shapse, *Chem. Rev.*, 1993, **93**, 861–885.
23 R. Dabrowski, P. Kula and J. Herman, High Birefringence Liquid Crystals, *Crystals*, 2013, **3**, 443–482.
24 Y. Iida, Y. Shimomura, M. Tokita and G. Konishi, Push-Pull biphenyl and tolane derivatives as novel luminescent liquid crystals: synthesis and properties, *Liq. Cryst.*, 2024, **51**, 2032–2045.
25 Y. Arakawa, Q. Ning, S. Karthick and S. Aya, Sulfur-based ferroelectric nematic liquid crystals, *J. Mater. Chem. C*, 2024, **12**, 16206–16217.
26 Y. Arakawa, S. Kang, J. Watanabe and G. Konishi, Assembly of thioether-containing rod-like liquid-crystalline materials assisted by hydrogen-bonding terminal carboxyl groups, *RSC Adv.*, 2015, **5**, 8056–8062.
27 S. Brown, E. Cruickshank, J. M. D. Storey, C. T. Imrie, D. Pociecha, M. Majewska, A. Makal and E. Gorecka, Multiple Polar and Non-polar Nematic Phases, *ChemPhysChem*, 2021, **22**, 2506–2510.
28 V. Borshch, Y.-K. Kim, J. Ziang, M. Gao, A. Jákli, V. P. Panov, J. K. Vij, C. T. Imrie, M.-G. Tambe, G. H. Mehl and O. D. Lavrentovich, Nematic twist-bend phase with nanoscale modulation of molecular orientation, *Nat. Commun.*, 2013, **4**, 2635.
29 G. H. Heilmeier, L. A. Zanoni and L. A. Barton, Gest-host interactions in nematic liquid crystals. A new electro-optic effect, *Appl. Phys. Lett.*, 1968, **13**, 91–92.
30 G. H. Heilmeier, Liquid crystal displays: An experiment in interdisciplinary research that worked, *IEEE Trans. Electron Devices*, 1976, **23**, 780–785.
31 R. G. Horn, J. N. Israelachvili and E. Perez, Forces due to structure in a thin liquid crystal film, *J. Phys.*, 1981, **42**, 39–52.

32 D. K. Sahu, S. Kol, S. Ramaswamy and S. Dhara, Omnidirectional transport and navigation of Janus particles through a nematic liquid crystal film, *Phys. Rev. Res.*, 2020, **2**, 032009.
33 A. Nych, J. Fukuda, U. Ognysta, S. Žumer and I. Muševič, Spontaneous formation and dynamics of half-skyrmions in a chiral liquid-crystal film, *Nat. Phys.*, 2017, **13**, 1215–1220.
34 I. Gharb, V. Palacio-Betancur, H. Ayeb, D. Demaile, J. J. de Pable, R. D. Kamien and E. Lacaze, Liquid Crystal Films as Active Substrates for Nanoparticle Control, *ACS Appl. Nano Mater.*, 2021, **4**, 6700–6708.
35 H. Coles and S. Morris, Liquid-crystal lasers, *Nat. Photonics*, 2010, **4**, 676–685.
36 M. Uchimura, Y. Watanabe, F. Araoka, J. Watanabe, H. Takezoe and G. Konishi, Development of laser dyes to realize low threshold in dye-doped cholesteric liquid crystal lasers, *Adv. Mater.*, 2010, **22**, 4473–4478.
37 X. Zhan, F.-F. Xu, Z. Zhou, Z. Zhou, Y. Yan, J. Yao and Y. S. Zhao, 3D Laser Displays Based on Circularly Polarized Lasing from Cholesteric Liquid Crystal Arrays, *Adv. Mater.*, 2021, **33**, 2104418.
38 T. M. Sarukhanyan, H. Gharagulyan, M. L. Sargsan, H. Grigoryan, R. S. Hakobyan, A. H. Gevorgyan and R. B. Alaverdyan, Lasing peculiarities in cholesteric multilayer structure with dye-doped polymer film depending on the concentration of laser dye and pumping energy, *Mol. Cryst. Liq. Cryst.*, 2020, **713**, 15–25.
39 S. Y. Cho, H. Yoshida and M. Ozaki, Emission Direction-Tunable Liquid Crystal Laser, *Adv. Opt. Mater.*, 2020, **8**, 200375.
40 J. Dziaduszek, R. Dabrowski, S. Urban, K. Garbat, A. Glushchenko and K. Czupryński, Selected fluorosubstituted phenyltolanes with a terminal group: NCS, CN, F, OCF3 and their mesogenic and dielectric properties and se for the formulation of high birefringence nematic mixtures to GHz and THz applications, *Liq. Cryst.*, 2017, **44**, 1277–1292.
41 M. Echeverri, I. Martín, A. Concellón, C. Ruize, M. S. Anselmo, E. Gutiérrez-Puebla, J. L. Sarrano and B. Gómez-Lor, Fluorescent and Electroactive Monoalkyl BTD-Based Liquid Crystals with Tunable Self-Assembling and Electronic Properties, *ACS Omega*, 2018, **3**, 11857–11864.
42 G. Liu, L. Ren, M. Zhang, S. Du, P. Chen, A. Gao, X. Chen and Z. An, Synthesis and properties of benzoxazole-based liquid crystals containing ethynyl group, *Liq. Cryst.*, 2020, **47**, 1719–1728.
43 S. K. Saha, G. Mohiuddin, M. K. Paul, S. P. Gupta, R. K. Khan, S. Chosh and S. K. Pal, Polar Switching and Cybotactic Nematic Ordering in 1,3,4-Thiadiazole-Based Short-Core Hockey Stick-Shaped Fluorescent Liquid Crystals, *ACS Omega*, 2019, **4**, 7711–7722.
44 J. Buchs, A. Geßner, B. Heyne, D. Janietz and H. Sawade, Fluorescent liquid crystals with rod-shaped π-conjugated hydrocarbon core, *Liq. Cryst.*, 2019, **46**, 281–298.
45 F. N. da Silva, A. S. da Silva, I. H. Bechtold, E. Zapp and A. A. Vieira, Luminescent liquid crystals based on 2,1,3-benzoxadiazole: conducive heterocycle or poor cousin of benzothiadiazole?, *Liq. Cryst.*, 2019, **46**, 1707–1717.
46 B. A. S. Jose, J. Yan and K. Akagi, Dynamic Switching of the Circularly Polarized Luminescence of Disubstituted Polyacetylene by Selective Transmission through a Thermotropic Chiral Nematic Liquid Crystal, *Angew. Chem., Int. Ed.*, 2014, **53**, 10641–10644.
47 J. Li, H. K. Bisoyi, J. Tian, J. Guo and Q. Li, Optically Rewritable Transparent Liquid Crystal Displays Enabled by Light-Driven Chiral Fluorescent Molecular Switches, *Adv. Mater.*, 2019, **31**, 1807751.
48 Y. Tsutsui, W. Zhang, S. Chosh, T. Sakurai, H. Yoshida, M. Ozaki, T. Akutagawa and S. Seki, Electrically Switchable Amplified Spontaneous Emission from Liquid Crystalline Phase of an AIEE-Active SEIPT Molecule, *Adv. Opt. Mater.*, 2020, **8**, 1902158.
49 W. Zhang, T. Sakurai, M. Aotani, G. Watanabe, H. Yoshida, V. S. Padalkar, Y. Tsutsui, D. Sakamaki, M. Ozaki and S. Seki, Highly Fluorescent Liquid Crystals from Excited-State Intramolecular Proton Transfer Molecules, *Adv. Opt. Mater.*, 2019, **7b**, 1801349.
50 Y. Tsutsui, T. Sakurai and S. Seki, Amplified spontaneous emission from a liquid crystalline phase: anisotropic property and active modulation, *Faraday Discuss.*, 2024, **250**, 271–280.
51 H. Chen, H. Yang, H. Kuo, W. Ko, K. Uchida and H. Yoshida, Photo-switching behaviour in liquid crystalline materials incorporating a non-planar dithienylcyclopentene core and their birefringence properties, *Liq. Cryst.*, 2022, **49**, 1475–1487.
52 M. Funahashi, Development of liquid-crystalline semiconductors with high carrier mobilities and their application to thin-film transistors, *Polym. J.*, 2009, **41**, 459–469.
53 H. Iino, T. Usui and J. Hanna, Liquid crystals for organic thin-film transistors, *Nat. Commun.*, 2015, **6**, 6828.
54 K. Sun, Z. Xiao, S. Lu, W. Zajaczkowski, W. Pisula, E. Hanssen, J. M. White, R. M. Williamson, J. Subbiah, J. Ouyang, A. B. Holmes, W. W. H. Wong and D. J. Jones, A molecular nematic liquid crystalline material for high-performance organic photovoltaics, *Nat. Commun.*, 2015, **6**, 6013.
55 G. Hu, M. R. Billa, S. P. Kitney and S. M. Kelly, Symmetrical carbazole-fluorene-carbazole nematic liquid crystals as electroluminescent organic semiconductors, *Liq. Cryst.*, 2018, **45**, 965–979.
56 D. Demus, One Century Liquid Crystal Chemistry: From Vorländer's Rods to Disks, Stars, and Dendrites, *Mol. Cryst. Liq. Cryst.*, 2006, **364**, 25–91.
57 Y.-M. Liao, N. Janarthanan, C.-S. Hsu, S. Gauza and S.-T. Wu, Synthesis and mesomorphic properties of fluoro and isothiocyanato biphenyl tolane liquid crystals, *Liq. Cryst.*, 2006, **33**, 1199–1206.
58 S. Kang, S. Nakajima, Y. Arakawa, G. Konishi and J. Watanabe, Large extraordinary refractive index in highly birefringent nematic liquid crystals of dinaphthyldiacetylene-based materials, *J. Mater. Chem. C*, 2013, **1**, 4222–4226.

59 J. P. Schroeder, Liquid Crystals: VII. Smectic-Nematic Transition Temperature as a Function of Alkyl End Group Length in *p*-Phenylene Di-*p*-*n*-alkoxynbenzoates, *Mol. Cryst. Liq. Cryst.*, 1980, **61**, 229–240.
60 E. Cruickshank, G. J. Strachan, J. M. D. Storey and C. T. Imrie, Chalcogen bonding and liquid crystallinity: Understanding the anomalous behaviour of the 4′-(alkylthio)[1,1′-biphenyl]-4-carbonitriles (*n*SCB), *J. Mol. Liq.*, 2022, **346**, 117094.
61 M. Hird, Fluorinated liquid crystals – properties and applications, *Chem. Soc. Rev.*, 2007, **36**, 2070–2095.
62 H. A. Ahmed, M. Hagar and O. A. Alhaddad, Mesomorphic and geometrical orientation study of the relative position of fluorine atom in some thermotropic liquid crystal systems, *Liq. Cryst.*, 2020, **47**, 404–413.
63 D. G. McDonnell, E. P. Raynes and R. A. Smith, Dipole moments and dielectric properties of fluorine substituted nematic liquid crystals, *Liq. Cryst.*, 2006, **6**, 515–523.
64 A. Chakraborty, B. Das, M. K. Das, S. Findeisen-Tandel, M.-G. Tamba, U. Baumeister, H. Kresse and W. Weissflog, New hockey stick compounds with a lateral methyl group showing nematic, synclinic and anticlinic smectic C phases, *Liq. Cryst.*, 2011, **38**, 1085–1097.
65 M. Hagar, H. A. Ahmed and O. A. Alhaddad, Experimental and theoretical approaches of molecular geometry and mesophase behaviour relationship of aterally substituted azopyridines, *Liq. Cryst.*, 2019, **46**, 1440–1451.
66 Y. Matsunaga and N. Miyajima, Effects of Branching of the Ester Alkyl Chain on the Liquid Crystalline Properties of Alkyl 4-(4-Alkoxybenzylideneamino)-benzoates, *Mol. Cryst. Liq. Cryst.*, 1985, **116**(3–4), 207–216.
67 Y. Shimomura, M. Tokita, A. Kawamura, J. Watanabe and G. Konishi, Fluorinated Poly(pentylene 4,4′-bibenzoate)e with Low Isotropization Temperatures and Unique Phase Transition Behavior, *Macromolecules*, 2023, **56**, 5152–5161.
68 R. Iwai, H. Yoshida, Y. Arakawa, S. Sasaki, Y. Iida, K. Igawa, T. Sakurai, S. Suzuki, M. Tokita, J. Watanabe and G. Konishi, Near-room temperature π-conjugated nematic liquid crystals in molecules with a flrxible seven-membered ring structure, *Aggregate*, 2025, **6**, e660.
69 S. Lou and G. C. Fu, Palladium/Tris(*tert*-butyl)phosphine-Catalyzed Suzuki Cross-Couplings in the Presence of Water, *Adv. Synth. Catal.*, 2010, **352**, 2081–2084.
70 J.-J. Shie and J.-M. Fang, Direct Conversion of Aldehydes to Amide, Tetrazoles, and Triazines in Aqueous Media by One-Pot Tandem Reactions, *J. Org. Chem.*, 2003, **68**, 1158–1160.
71 N. Miyaura, T. Ishiyama, H. Sasaki, M. Ishikawa, M. Sato and A. Suzuki, Palladium-catalyzed inter- and intramolecular cross-coupling reactions of B-alkyl-9-borabicyclo[3.3.1]nonane derivatives with 1-halo-1-alkenes of haloarenes. Synthesis of functionalized alkenes, arenes, and cycloalkenes *via* a hydroboration-coupling sequence, *J. Am. Chem. Soc.*, 1989, **111**, 312–321.
72 N. Miyaura and A. Suzuki, Palladium-catalyzed cross-coupling reactions of organoboron compounds, *Chem. Rev.*, 1994, **94**, 2457–2483.
73 A. Sen and Y. M. A. Yamada, Latest Developments on Palladium- and Nickel-Catalyzed Cross-Couplings Using Aryl Chlorides: Suzuki–Miyaura and Buchwald–Hartwig Reactions, *Synthesis*, 2024, 3555–3574.
74 T. Tanaka, A. Matsumoto, A. S. Klymchenko, E. Tsurumaki, J. Ikenouchi and G. Konishi, Fluorescent Solvatochromic Probe for Long-Term Imaging of Lipid Order in Living Cells, *Adv. Sci.*, 2004, **11**, 2309721.
75 R. Iwai, S. Suzuki, S. Sasaki, A. S. Sairi, K. Igawa, T. Suenobu, K. Morokuma and G. Konishi, Bridged Stilbenes: AIEgens Designed via a Simple Strategy to Control the Non-radiative Decay Pathway, *Angew. Chem., Int. Ed.*, 2020, **59**, 10566–10573.
76 Y. Shimomura, K. Igawa, S. Sasaki, N. Sakakibara, R. Goseki and G. Konishi, Flexible Alkylene Bridges as a Tool to Engineer Crystal Distyrylbenzene Structures Enabling Highly Fluorescent Monomeric Emission, *Chem. – Eur. J.*, 2022, **28**, e202201884.
77 Y. Shimomura and G. Konishi, Push-Pull Bridged Distyrylbenzene with Highly Bright Solid-State Red-Orange Aggregation-Induced Emission, *Chem. – Eur. J.*, 2023, **29**, e202301191.
78 G. Konishi, Y. Sawatari, R. Iwai, T. Tanaka, Y. Shimomura and M. Tokita, Synthesis of Side-Chain Liquid Crystalline Polyacrylates with Bridged Stilbene Mesogens, *Molecules*, 2024, **29**, 5220.
79 Y. Arakawa, S. Nakajima, R. Ishige, M. Uchimura, S. Kang, G. Konishi and J. Watanabe, Synthesis of diphenyldiacetylene-based nematic liquid crystals and their high birefringence properties, *J. Mater. Chem.*, 2012, **22**, 8394–8398.
80 Y. Arakawa, S. Kang, H. Tsuji, J. Watanabe and G. Konishi, The design of liquid crystalline bistolane-based materials with extremely high birefringence, *RSC Adv.*, 2016, **6**, 92845–92851.
81 Y. Arakawa, S. Kang, H. Tsuji, J. Watanabe and G. Konishi, Development of novel bistolane-based liquid crystalline molecules with an alkylsulfanyl group for highly birefringent materials, *RSC Adv.*, 2016, **6**, 16568–16574.
82 I. Haller, Thermodynamic and static properties of liquid crystals, *Prog. Solid State Chem.*, 1975, **10**, 103–118.
83 M. Krämer, U. H. F. Bunz and A. Dreuw, Comprehensive Look at the Photochemistry of Tolane, *J. Phys. Chem. A*, 2017, **121**, 946–953.
84 J. Kobayashi, H. Yoshida and M. Ozaki, Planar optics with patterned chiral liquid crystals, *Nat. Photonics*, 2016, **10**, 389–392.
85 S. Y. Cho, M. Takahashi, J. Fukuda, H. Yoshida and M. Ozaki, Directed self-assembly of soft 3D photonic crystals for holograms with omnidirectional circular-polarization selectivity, *Commun. Mater.*, 2021, **2**, 39.
86 W. Haase, H. Paulus, Z. X. Fan, I. H. Ibrahim and M. Mokhles, The Crystal and Molecular Structure of the mesogenic 4-Cyano-4′-*n*-pentyl-*p*-terphenyl (T15) and its Solid State Polymorphism, *Mol. Cryst. Liq. Cryst., Lett.*, 1988, **6**, 113–121.

87 M. J. Frisch, G. W. Trucks, H. B. Schlegel, G. E. Scuseria, M. A. Robb, J. R. Cheeseman, G. Scalmani, V. Barone, G. A. Petersson, H. Nakatsuji, X. Li, M. Caricato, A. V. Marenich, J. Bloino, B. G. Janesko, R. Gomperts, B. Mennucci, H. P. Hratchian, J. V. Ortiz, A. F. Izmaylov, J. L. Sonnenberg, D. Williams-Young, F. Ding, F. Lipparini, F. Egidi, J. Goings, B. Peng, A. Petrone, T. Henderson, D. Ranasinghe, V. G. Zakrzewski, J. Gao, N. Rega, G. Zheng, W. Liang, M. Hada, M. Ehara, K. Toyota, R. Fukuda, J. Hasegawa, M. Ishida, T. Nakajima, Y. Honda, O. Kitao, H. Nakai, T. Vreven, K. Throssell, J. A. Montgomery, Jr., J. E. Peralta, F. Ogliaro, M. J. Bearpark, J. J. Heyd, E. N. Brothers, K. N. Kudin, V. N. Staroverov, T. A. Keith, R. Kobayashi, J. Normand, K. Raghavachari, A. P. Rendell, J. C. Burant, S. S. Iyengar, J. Tomasi, M. Cossi, J. M. Millam, M. Klene, C. Adamo, R. Cammi, J. W. Ochterski, R. L. Martin, K. Morokuma, O. Farkas, J. B. Foresman and D. J. Fox, *Gaussian 16, Revision C.01*, Gaussian, Inc., Wallingford CT, 2016.

88 D. W. Bruce, K. Heyns and V. Vill, Vorlander's wheel, *Liq. Cryst.*, 1997, **23**, 813–819.

89 S. Kapuściński, J. Szczytko, D. Pociecha and P. Kaszyński, Mesogenic Behavior of a 6-Oxoverdazyl Diradical: Towards Organic High-Spin Liquid Crystals, *Mater. Chem. Front.*, 2024, **8**, 1112–1119.

90 S. Cao, C. Liu and M. Yoshio, *Mater. Chem. Front.*, 2023, **7**, 2828–2838.

91 K. Sambe, T. Takeda, N. Hoshino, W. Matsuda, K. Shimada, K. Tsujita, S. Maruyama, S. Yamamoto, S. Seki, Y. Matsumoto and T. Akutagawa, Carrier Transport Switching of Ferroelectric BTBT Derivative, *J. Am. Chem. Soc.*, 2024, **146**, 8557–8566.

92 S. Ishikawa, K. Yamasumi, S. Sugiura, S. Sato, G. Watanabe, Y. H. Koo, S. Seki, Y. Bando, Y. Haketa, H. Shinokubo and H. Maeda, Norcorroles as antiaromatic π-electronic systems that form dimension-controlled assemblies, *Chem. Sci.*, 2024, **15**, 7603–7609.

93 Y. Kobayashi, A. Muranaka, K. Kato, A. Saeki, T. Tanaka, M. Uchiyama, A. Osuka, T. Aida and T. Sakurai, A structural parameter to link molecular geometry to macroscopic orientation in discotic liquid crystals: study of metalloporphyrin tapes, *Chem. Commun.*, 2021, **57**, 1206–1209.

94 K. Igeta, A. Higuchi, J. Kobashi, Y. Tomioka, S. Oka and H. Yoshida, *ACS Appl. Opt. Mater.*, 2024, **2**, 1314–1320.

95 G. Washio, T. Kajitani, S. Nishimura and A. Shishido, Design of ionic liquid crystals enabled by [2]rotaxane structure formation, *Mol. Syst. Des. Eng.*, 2024, **9**, 826–831.

96 Y. Arakawa, S. Sasaki, K. Igawa, M. Tokita, G. Konishi and H. Tsuji, Birefringence and photoluminescence properties of diphenylacetylene-based liquid crystal dimers, *New J. Chem.*, 2020, **44**, 17531–17541.

97 C. Anders, T. Tan, V.-M. Fischer, R. Wang, M. Alaasar, R. Waldecker, Y. Cao, F. Liu and C. Tschierske, Engineering "Meso-Atom" Bonding: Honeycomb-Network Transitions in Reticular Liquid Crystals, *Aggregate*, 2025, e728(Early View).

98 Z. Deng, X. Chen, X. Deng, J. Yang, S. Zhou, J. Chen, P. Wang, H. Yang and R. Lan, Programmable light-driven soft actuator enabled by structurally anisotropic liquid crystalline network, *Aggregate*, 2025, **6**, e633.

99 Y. He, J. Zhang, C. Ma, J. Liu, J. Guo, T. Han, R. Hu, B. S. Li and B. Z. Tang, Multifaceted regulation of chiroptical properties and self-assembly behaviors of chiral fluorescent polymers, *Aggregate*, 2024, **5**, e642.

100 Y. Sawatari, Y. Shimomura, M. Takeuchi, R. Iwai, T. Tanaka, E. Tsurumaki, M. Tokita, J. Watanabe and G. Konishi, Supramolecular liquid crystals from the dimer of L-shaped molecules with tertiary amide end groups, *Aggregate*, 2024, **5**, e507.

